



HAL
open science

Spin waves in fractals

Pascal Monceau, Jean-Claude Serge Lévy

► **To cite this version:**

Pascal Monceau, Jean-Claude Serge Lévy. Spin waves in fractals. Jean-Claude Serge Lévy. Nanostructures and their magnetic properties, Research Signpost, pp.227-256, 2009. hal-00521373

HAL Id: hal-00521373

<https://hal.science/hal-00521373>

Submitted on 28 Jun 2023

HAL is a multi-disciplinary open access archive for the deposit and dissemination of scientific research documents, whether they are published or not. The documents may come from teaching and research institutions in France or abroad, or from public or private research centers.

L'archive ouverte pluridisciplinaire **HAL**, est destinée au dépôt et à la diffusion de documents scientifiques de niveau recherche, publiés ou non, émanant des établissements d'enseignement et de recherche français ou étrangers, des laboratoires publics ou privés.



Distributed under a Creative Commons Attribution 4.0 International License

Spin waves in fractals

Pascal Monceau^{1,2} and Jean-Claude Serge Lévy³

¹Laboratoire Matière et Systèmes Complexes (MSC)
UMR 7057 CNRS et Université Paris Diderot

²Département de Physique et Modélisation
Université d'Evry-Val d' Essonne

Boulevard F. Mitterrand 91025 Evry France

³Laboratoire Matériaux et Phénomènes Quantiques (MPQ)

UMR 7162 CNRS et Université Paris Diderot

10 rue Alice Domont et Léonie Duquet

75013 Paris France

Abstract : Spin wave frequencies and profiles of several Sierpinski Carpets taken at different iteration levels are calculated. Spin wave spectra of these fractals with short ranged ferromagnetic exchange are found to be singular continuous functions of the frequency with quite numerous steps and cliffs, i.e. energy gaps and degenerate modes, resulting in devil's staircase spectra. The study of connectivity reveals the existence of several different connectivity areas within each fractal. It marks mode localization and symmetry. Spin wave modes are found to be quite sensitive to fractal topology and connectivity as already observed about critical properties of fractals. The extension of the properties of magnetic excitations, first to random fractals, then to elastic waves as well as to electronic states in fractals is introduced. Applications to spin wave resonance in dilute magnetic semiconductors are discussed.

P.A.C.S.: 61.43.Hv, 75.30.Ds, 75.40.Mg, 75.50.Ph

1. Introduction

Quite numerous physical objects evidence simultaneously continuous and discontinuous properties. There is now the typical example of low temperature 2D deposits made of numerous dendrites and islands with internal seas and islands of various shapes exhibiting several hierarchical levels [1]. It follows the already classic observations of percolation clusters [2] and of large clusters due to Diffusion Limited Aggregation, (DLA) [3]. During the seventies, B. Mandelbrot classified such Cantor-like materials with the notion of fractals [4], now commonly used for such materials. A first preliminary question concerns the nature of fractal materials and how they can be produced. A second preliminary question on these new materials deals with their theoretical properties. These properties were intensively studied

soon after their naming, with for instance the idea of fractons associated with low frequency modes of these materials [5]. Practically, a more prosaic question concerns the present experimental status of fractals and their applications. So, the definition of the scope of this paper requires preliminary short answers to these three main questions.

1.1. Fractal materials

The nice definition of fractals by Mandelbrot generalizes that of Cantor sets [6] and similar sets (embedded in two or three-dimensional spaces) such as Von Koch, Sierpinski or Menger sets. Mandelbrot took advantage of Hausdorff's measure [7] and applied it to the classification of these continuous-discontinuous objects. Physically, the observation of numerous percolating systems where an infinite connected set of one component appears in a multicomponent material [2] was among the first strong evidence for the existence of fractal materials, since percolating clusters exhibit hierarchical properties just as Cantor sets do. The study of Diffusion Limited Aggregation was another evidence for fractals, both from simulation and experiment [3]; infinite DLA clusters obviously evidence percolation, so that percolating systems play a central part in the initial studies of fractals. Low temperature deposits [1] or solidifications [8] create also out of equilibrium properties which are due to weak diffusion. These slowly varying structures exhibit hierarchical properties since, in this low density matter, atomic clusters are made of a few interacting atoms, and atomic clusters interact between themselves as atoms do, up to a numerical factor. More complex clusters are made of a few simple clusters and the interactions between atoms, atomic clusters or complex clusters is the same except for intensity which is proportional to the square of the number of involved atomic units. Thus there is a natural geometric hierarchy among these structures. Low temperature deposits at different low concentrations enabled numerous authors [1, 8] to evidence fractals with any fractal dimension as also observed from numerical simulation [9]. These examples already give practical rules for producing fractals of arbitrary dimensions according to convenient temperatures and initial concentration for the generating system. Whereas the symmetry associated with crystalline materials is translation invariance, it should be emphasized that hierarchical properties of fractals are closely linked to scale invariance.

1.2. Fractal properties

The first known properties of fractals are their structural properties arising from their definition. Fractals are hierarchical structures with intermediate density dimensions [4].

Deterministic and random fractals have hierarchical, self-similar connectivity properties as well as lacunarity properties [10, 11].

A second class of fractal properties concerns the excitation spectrum of these structures, where hierarchical properties have been noted, with the definition of dynamic exponents for classifying fractons, i.e. low frequency modes [5, 12]. In the present paper we will be interested in the magnetic excitation spectrum of fractal objects in a more applied way by considering their whole excitation spectrum and not only the low frequency modes which can evidence the fracton property. The whole excitation spectrum is known to be a singular continuous excitation spectrum with quite numerous energy gaps in the case of self similar objects [13] as it also occurs for aperiodic systems and quasicrystals [14] which also evidence an at least approximate self similarity [15]. So, a singular continuous spectrum is expected in the case of fractals.

A third property of interest of these fractal materials is their critical behaviour [16] since universality classes associated to second order phase transitions are known to depend on space dimensionality. In the field of critical phenomena, ϵ -expansions yield critical exponents associated with second order phase transitions in non-integer dimensions. The question of the physical meaning of these expansions leads naturally to deal with fractals, which can be used to generate a nearly continuous dimensionality variation. As a main result, it has been shown [16, 17] that the usual statement of universality does not hold in the case of fractals. Although the hyperscaling relation is satisfied when the space dimension is replaced by the Hausdorff one, the set of critical exponents cannot be provided by ϵ -expansions since it does not only depend upon the Hausdorff dimension, the symmetry of the order parameter and the interaction range but also upon topological features of the fractal. The critical behaviour of discrete symmetry spin models on fractals is said to be understood in the framework of weak universality. It should be kept in mind that translation invariance is a necessary condition to proceed with dimensional perturbations; thus ϵ -expansions are based upon hypothetical translationally invariant lattices with a non-integer dimension. Hence, the disagreements between ϵ -expansions and Monte-Carlo results can be attributed to the translation symmetry breaking in fractal systems. The influence of the topological features of the fractal structure, which are present at any scale, on the critical behaviour can hence be understood as an additional field related to a kind of disorder; this disorder should be understood as a deviation from the translational symmetry. So, the study of phase transitions in fractals by renormalization group and by numerical simulation has been useful for a better understanding of phase transitions in a much more general scope [17]. Of course the existence of connected

sets within fractals, i.e. percolation within fractals is also a basic question for the study of phase transitions in fractals, so percolation on fractal sets was also studied [11] and revealed the existence of $d - 1$ different levels of percolation in d dimensions, i.e. several levels of percolation.

1.3. Experiments with fractals.

There are many practical interests in fractals : For instance dilute magnetic impurities in semiconductors, where impurity network designs more or less fractal sets, define magnetic semiconductors. These magnetic semiconductors have typical semiconductor conductivity and are well fitted for integrated semiconductor electronic devices. These materials are also magnetic materials and thus could be used in giant magneto resistance (GMR) circuitry [18] directly with semiconductor electronics. Magnetic resonance has already been studied in these materials and has evidenced new properties [19]. Since dilution and fractal structural properties can be easily varied in magnetic semiconductors, the complete adaptability of these materials is obvious. As a matter of fact, magnetic couplings in semiconductors have also a non local part with the classical examples of Ruderman-Kittel-Kasuya-Yosida (RKKY) long ranged interaction [20] and dipole-dipole interaction [21] which is also long ranged. So, different kinds of magnetic modes must be distinguished according to respective interaction ranges. The nature of the connectivity to be accounted for such impurity networks is not the same for these different kinds of modes.

Historically, fractal properties have been evidenced at the dielectric breakdown, when an electric current can go through percolating conductive particles located within an insulating media [22]. This famous abrupt transition between an isolating state and a conductive state can be easily controlled by various phenomena. That conductivity phenomenon could provide a lot of applications comparable to the numerous applications of Zener avalanche breakdown diodes [23] since it is well fitted for electronic applications.

Of course, elastic properties of alloys or defected materials show a similar abrupt transition between a more or less rigidly connected state and a smooth non-connected state when looking around percolation of the more rigid species. These transitions depend on species concentration. For fractal sets, these transitions between hard and soft behaviours depend on the fractal dimension of these sets. The static elastic properties of fractal materials have also their dynamic counterparts for phonons which have special excitation spectra [13]. So fractal materials are already ready to be used for numerous applications.

The goal of the present paper is to analyze the magnetic excitation spectra of fractal materials. It can help when analyzing spin wave resonance in fractals as already observed experimentally [19]. This spectral knowledge can be also used for designing optimal materials for magnonics, i.e. special magnetic wave propagation within tailored magnetic systems [24], by revealing energy spectrum gaps, i.e. selected frequency bands which are reflected when facing fractals. Further advances issued from the study of spin waves in fractals consist in understanding the magnetic thermal behaviour of such magnetic fractals as well as magnetization reversal in fractals. Of course these behaviours are dominated by long wavelength modes, i.e. the fracton branch, but since this fracton branch is quite depleted in front of the magnon branch of a full sample, the contribution of higher modes cannot be neglected. Magnetic properties are emblematic of more general physical properties. From that point of view, the present study is also introductive for electronic and elastic properties of fractals.

A first section of this paper is devoted to the general properties of fractal structures, the principles of calculation of these properties for several fractal structures, and the so deduced results. A final section is devoted to the comments and conclusions as well as on the perspectives opened for excitations in fractals.

2. Generalities

2.1. Fractal Structures; random and deterministic fractals.

Most experiments deal with random fractals as they occur in percolating systems or with low temperature deposits. Most of theoretical treatments deal with deterministic fractals using deterministic inflation rules, for calculation convenience: deterministic fractals keep the hierarchical properties, the scale invariance is not statistical and thus does not need to be averaged over a set of structures as in random fractals. From now on, we will deal with fractals constructed by iteration of an initial generating cell, whose symmetry is thus the Discrete Scale Invariance (DSI). Strictly speaking, it should be emphasized that a true fractal structure is obtained when the number of iteration steps of the generating cell tends towards infinity. Fig. 1 shows the fourth step of iteration ($k=4$) of a Random Sierpinski Carpet embedded in a two-dimensional space, where at each iteration level, $p=13$ subsquares chosen in a random way are kept among the $n^2 = 4^2 = 16$ possible ones of the generating cell. This structure, called RSC(4, 13, 4), has a fractal dimension $d_f = (\ln 13)/(\ln 4) \cong 1.850$. Let us

recall that the fractal dimension relates the “mass” of the fractal, i. e. the total number of elementary squares $N = p^k$, to its linear size $L = n^k$, since $N = L^{d_f}$.

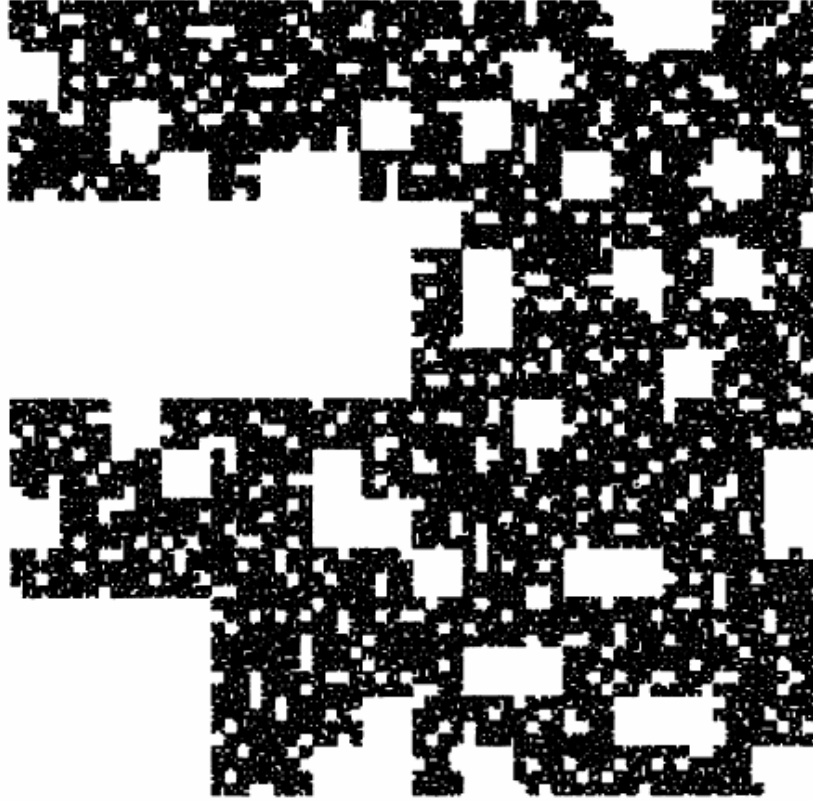


Fig. 1. Random Sierpinski Carpet at the fourth iteration level $k = 4$: RSC(4, 13, 4) with $d_f \approx 1.850$

There is a strong evidence for a large distribution of both occupied and unoccupied lengths in the Random Sierpinski Carpet shown in Fig. 1. For the simplicity of future calculations it is useful to introduce deterministic fractal structures $SC(n,p,k)$ where p subsquares among n^2 available subsquares are occupied in a deterministic way; the fractal dimension $d_f = \ln p / \ln n$ can be easily varied by conveniently choosing the numbers p and n . Furthermore, the geometrical choice of the p occupied subsquares within an initial square enables us to vary the connectivity parameters, i.e. the connectivity subdimensions evidenced from the eigenvalues of connectivity matrix [11]. So, for a given fractal dimension, quite different topologies associated with different values of connectivity subdimensions can be obtained on these deterministic fractals. For comparison with the random Sierpinski carpet shown in Fig. 1, a deterministic Sierpinski Carpet denoted $SC_a(4, 12, 4)$ at the same fourth

level of iteration is shown in Fig. 2; the subscript letter *a* refers to the way the four deleted subsquares are chosen in the generating cell, namely the center in the present case.

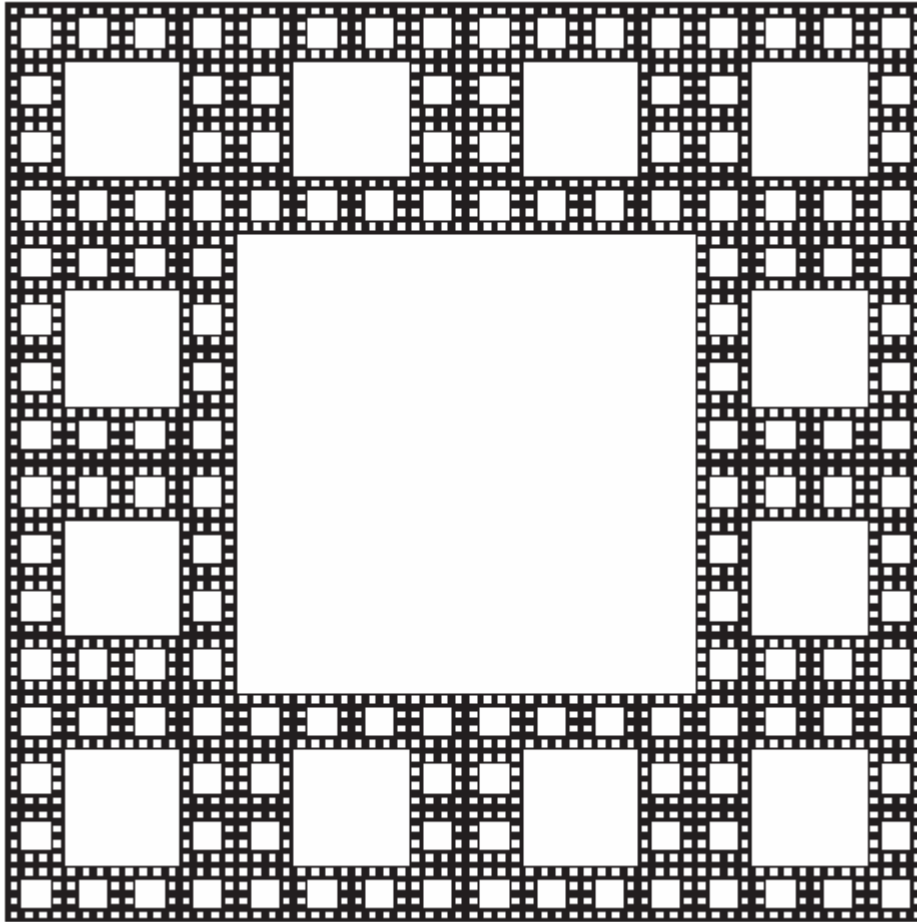


Fig. 2. A deterministic Sierpinski Carpet at iteration level $k = 4$: $SC_a(4, 12, 4)$ with $d_f \approx 1.792$

As already noticed in the case of a random Sierpinski Carpet shown in Fig. 1, there is also a large distribution of segment lengths in the deterministic Sierpinski Carpet of Fig. 2. The study of deterministic fractal structures can be a good approach of more realistic random fractal structures. In order to visualize the topology of this deterministic set, the first level of iteration of the set represented in Fig. 2, i.e. the generating cell, is shown in Fig. 3. This generating cell is compared here with another one which generates Sierpinski Carpets sharing the same fractal dimension and the square symmetry: $SC_b(4, 12, 4)$.

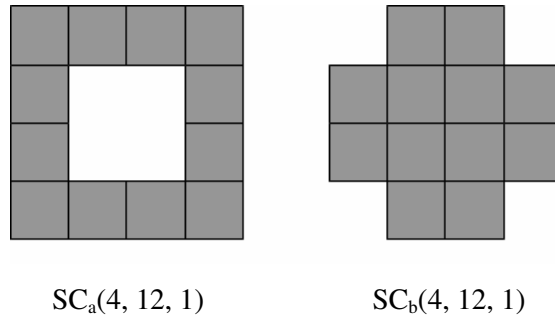


Fig. 3. The first iteration step of the Sierpinski Carpet of Fig. 2: $SC_a(4, 12, 1)$ compared to: $SC_b(4, 12, 1)$. The generated Sierpinski Carpets share the fractal dimension $d_f \approx 1.792$, but have different connectivities

The first step of other Sierpinski Carpets $SC(5, 16, 1)$ embedded in a two-dimensional space with square symmetry and sharing the same fractal dimension $d_f = (\ln 16)/\ln 5 \approx 1.723$ is shown in Fig. 4. The magnetic properties of these structures will also be considered within this paper.

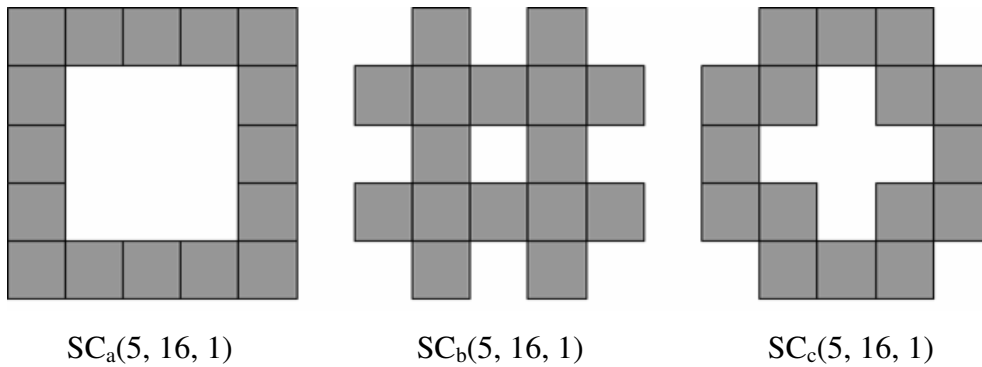


Fig. 4. The first iteration step of Sierpinski Carpets with different connectivities : $SC_a(5, 16, 1)$, $SC_b(5, 16, 1)$, and $SC_c(5, 16, 1)$. These structures share the same fractal dimension $d_f \approx 1.723$

The first iteration step of Sierpinski Structures (often called Menger fractals) embedded in a three-dimensional space with cubic symmetry sharing the same fractal dimension $d_f = \ln p/\ln n \approx 2.904$ is shown in Fig. 5. As noticed before in Figs 3 and 4, two initial structures with here a cubic symmetry can be designed as shown in Fig. 5.

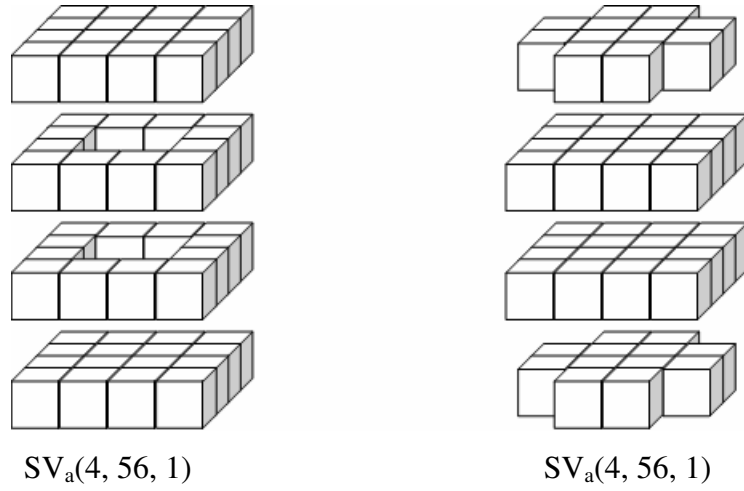


Fig. 5. The first iteration step of Sierpinski Structures embedded in a three dimensional space with different connectivities: $SV_a(4, 56, 1)$ and $SV_b(4, 56, 1)$ share the same fractal dimension $d_f \approx 2.904$

The names given to these structures follow the same rules as before, namely SC for Sierpinski Carpets, SV for Menger structures, and the index is used to characterize different geometric distributions of the deleted subsquares in a generating cell. These SC and SV structures are invariant under square or cubic symmetry respectively, whatever the iteration step.

2.2. Structural Properties: Connectivity matrix of fractals

2.2.1. Connectivity in fractals: general properties

At the intersection of column α and line β , the connectivity matrix has for element the number $n_{\alpha\beta}$ of objects of a given connectivity α deduced from the iteration step starting from an object with connectivity β . This gives the connectivity matrix element: $C_{\alpha\beta} = n_{\alpha\beta}$ of the connectivity matrix \mathbf{C} . In the case of Sierpinski Carpets embedded in a two-dimensional space with square symmetry, the different states of connectivity taking in account only the first neighbours represented on Fig. 6 are respectively (0) i.e. an isolated square, (1) i.e. a single neighbor, (2L) i.e. two neighbours at a right angle, (2-) i.e. two neighbours aligned along a line, (3) and (4) [11]. This enables us to define a 6x6 connectivity matrix \mathbf{C} .

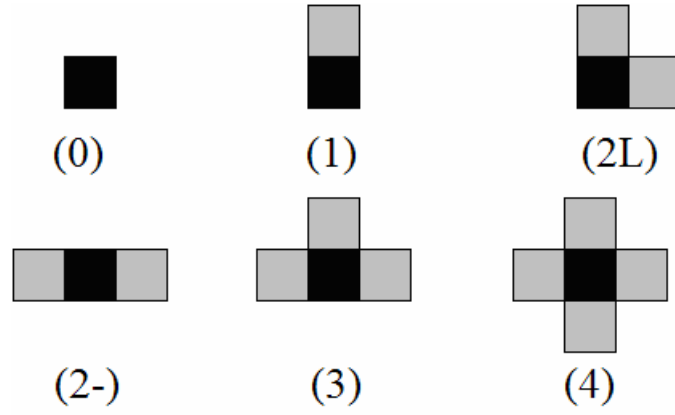


Fig. 6. The six connectivity states of a given site (in black) in the case of Sierpinski Carpets embedded in a two-dimensional space with square symmetry.

Quite obviously, from this very definition, the connectivity matrix has the properties of a transfer matrix, i.e. the number of objects of connectivity class α deduced after k iteration steps when starting from the initial state denoted by the vector \mathbf{i} is given by the line α of the vector $\mathbf{C}^k \mathbf{i}$. Hence, the eigenvalues of the connectivity matrix \mathbf{C} are meaningful. After a large number of iterations, only fractal properties remain, so that the highest eigenvalue of the connectivity matrix is linked with the fractal dimension. This eigenvalue is the number of retained objects at each step. So, the other eigenvalues s_i of the connectivity matrix are also linked with corrective subdimensions d_i [11] where $d_i = \ln s_i / \ln n$.

2.2.2. Connectivity in Sierpinski Carpets SC embedded in a two-dimensional space

For each of the symmetric deterministic structures introduced before, the connectivity matrix, its eigenvalues s_i , and the associated dimensions $d_i = (\ln s_i) / (\ln n)$ defined from the transfer matrix can be easily calculated. In the case of random fractals, the elements $\mathbf{C}_{\alpha\beta}$ can be obtained from complicated combinatorial calculations [11]. The highest dimension is the fractal dimension $d_f = (\ln p) / (\ln n)$. The subdimensions provide a direct connectivity classification of these different structures [11].

In the case $\text{SC}_a(4, 12, k)$ shown in Fig. 2 and 3, the connectivity matrix $\mathbf{C}_{a,4,12}$ reads:

$$\mathbf{C}_{a,4,12} = \begin{pmatrix} 0 & 0 & 4 & 8 & 0 & 0 \\ 0 & 0 & 2 & 6 & 4 & 0 \\ 0 & 0 & 1 & 4 & 6 & 1 \\ 0 & 0 & 0 & 4 & 8 & 0 \\ 0 & 0 & 0 & 2 & 8 & 2 \\ 0 & 0 & 0 & 0 & 8 & 4 \end{pmatrix} \quad (1)$$

Its eigenvalues are 12, 4 and 1. The highest eigenvalue of this connectivity matrix gives the fractal dimension of this set, $d_f = \ln 12 / \ln 4 \cong 1.792$, while the second dimension gives the connectivity subdimension $d_1 = \ln 4 / \ln 4 = 1$ which is obviously the dimension of the interface line. The last subdimension $d_2 = \ln 1 / \ln 4 = 0$ is the dimension of an isolated corner point.

For the other symmetric Sierpinski Carpet with 4 deleted corners, $\text{SC}_b(4, 12, k)$ shown in Fig. 3, which has the same fractal dimension as $\text{SC}_a(4, 12, k)$ but a different topology, the connectivity matrix $\mathbf{C}_{b,4,12}$ is quite different from the previous matrix $\mathbf{C}_{a,4,12}$, and reads:

$$\mathbf{C}_{b,4,12} = \begin{pmatrix} 0 & 0 & 8 & 0 & 0 & 4 \\ 0 & 0 & 6 & 0 & 2 & 4 \\ 0 & 0 & 4 & 0 & 4 & 4 \\ 0 & 0 & 4 & 0 & 4 & 4 \\ 0 & 0 & 2 & 0 & 6 & 4 \\ 0 & 0 & 0 & 0 & 8 & 4 \end{pmatrix} \quad (2)$$

Its eigenvalues are 12 and 2. The highest eigenvalue still gives the fractal dimension $d_f = \ln 12 / \ln 4$ as expected, while the second dimension gives the connectivity subdimension $d_1 = \ln 2 / \ln 4 = 1/2$ which is obviously the dimension of a segmented line, i.e. a Cantor set where two squares are retained among four, as it occurs on the edge of this Sierpinski Carpet. These examples already show that connectivity subdimensions are sensitive to topology. Connectivity subdimensions give a fractal measure of the interfaces.

In the case of Sierpinski Carpets with $n=5$, Fig. 4 shows three different first iteration steps with the same number (sixteen) of retained squares: $\text{SC}_i(5, 16, 1)$, with i is equal to a, b or c. Their connectivity matrices are obviously 5x5 matrices or lower rank matrices since isolated squares are never produced. The so-reduced connectivity matrices are respectively:

$$\mathbf{C}_{a,5,16} = \begin{pmatrix} 1 & 6 & 8 & 1 \\ 0 & 6 & 10 & 0 \\ 3 & 0 & 11 & 2 \\ 0 & 0 & 12 & 4 \end{pmatrix} \quad \mathbf{C}_{b,5,16} = \begin{pmatrix} 6 & 6 & 4 \\ 4 & 8 & 4 \\ 0 & 12 & 4 \end{pmatrix} \quad \mathbf{C}_{c,5,16} = \begin{pmatrix} 8 & 2 & 6 \\ 8 & 2 & 6 \\ 6 & 1 & 9 \end{pmatrix} \quad (3)$$

Their eigenvalues are respectively:

a) $SC_a(5, 16, k)$: 16, 5 and $\frac{1 \pm i\sqrt{23}}{2}$, a pair of conjugate complex eigenvalues.

b) $SC_b(5, 16, k)$: 16 and 2.

c) $SC_c(5, 16, k)$: 16 and 3.

Apart from the fractal dimension $d_f = \ln 16 / \ln 5 \cong 1.723$ always found, the fractal dimension of the interface is found as a subdimension, respectively:

case a) : $d_1 = 1$ the line dimension

case b): $d_1 = \ln 2 / \ln 5 \cong 0.431$

case b): $d_1 = \ln 3 / \ln 5 \cong 0.683$

In cases b) and c) these subdimensions are the dimensions of the Cantor sets which appear at the edge of these Sierpinski Carpets.

A practical numerical case of interest lies in $SC_a(3, 8, k)$, a Sierpinski Carpet with a central hole. The reduced connectivity matrix $C_{3,8}$ of $SC_a(3, 8, k)$ reads:

$$C_{3,8} = \begin{pmatrix} 1 & 2 & 4 & 1 \\ 0 & 2 & 6 & 0 \\ 0 & 1 & 5 & 2 \\ 0 & 0 & 4 & 4 \end{pmatrix} \quad (4)$$

Its eigenvalues are 8, 3 and 1. Apart from the fractal dimension $d_f = \ln 8 / \ln 3 \cong 1.893$, its subdimensions are 1 and 0, i.e. the line dimension and the point dimension respectively. These are the same subdimensions as for $SC_a(4, 12, k)$ and $SC_a(5, 16, k)$ because interfaces are also the full interface line and the corner point.

2.2.3. Connectivity in Menger fractals SV embedded in a three-dimensional space

In the case of Menger fractals SV which are invariant under cubic symmetry, the different states of connectivity are respectively: (0) i.e. a single isolated cube, (1) i.e. one neighbouring cube, (2L) i.e. two neighbours at a right angle, (2-) i.e. two neighbours aligned along a line, (3C), i.e. a corner at a cube apex, (3P) i.e. three neighbours in a plane, (4P) four neighbours in a plane, (4T) tetrahedron of four neighbours, (5) five neighbours and (6) six neighbours. These connectivity states enable to define a 10x10 connectivity matrix C .

In the case of the structures defined in Fig. 5 by $SV_a(4, 56, 1)$ and $SV_b(4, 56, 1)$, the reduced connectivity matrices are respectively:

$$\mathbf{C}_{a,4,56} = \begin{pmatrix} 1 & 12 & 9 & 27 & 7 \\ 0 & 8 & 0 & 40 & 8 \\ 0 & 8 & 4 & 32 & 14 \\ 0 & 4 & 0 & 32 & 20 \\ 0 & 0 & 0 & 24 & 32 \end{pmatrix} \quad \mathbf{C}_{b,4,56} = \begin{pmatrix} 6 & 12 & 18 & 20 \\ 2 & 12 & 18 & 24 \\ 0 & 8 & 20 & 28 \\ 0 & 0 & 24 & 32 \end{pmatrix} \quad (5)$$

Once more, the rank reduction is due to the fact that some states of connectivity are never produced. The connectivity matrix eigenvalues are respectively:

- a) $\text{SV}_a(4, 56, 1)$: 56, 16, 4 and 1.
- b) $\text{SV}_b(4, 56, 1)$: 56, 12 and 2.

This defines the fractal dimension $d_f = \ln 56 / \ln 4 \cong 2.904$ and the respective subdimensions:

Case a) 2, 1 and 0;

Case b) $d_1 = \ln 12 / \ln 4 \cong 1.792$ and $1/2$.

In both cases, the interface dimension found as the first subdimension is $d_1 = 2$ for $\text{SV}_a(4, 56, k)$ and $d_1 = \ln 12 / \ln 4 \cong 1.792$ for $\text{SV}_b(4, 56, k)$ which turns out to be the dimension of the interface $\text{SC}_b(4, 12, k)$ of $\text{SV}_b(4, 56, k)$.

So, connectivity subdimensions are sensitive to the interface properties and complete the global approach of fractal dimension.

2.3. Spin Hamiltonian and spin waves modes in fractals

2.3.1. Spin Hamiltonian and spin-waves eigenproblem

From the fractal objects previously constructed by squares and cubes, sets of points f are defined by putting a point at the centre of each occupied elementary square or cube. The previously defined connectivity now selects the nearest neighbours of an occupied site. A spin is placed at each point of the set, and the simplest spin Hamiltonian to be considered reads:

$$H = -\frac{1}{2} \sum_{f,g,\alpha} J_{f,g,\alpha} S_f^\alpha S_g^\alpha - g\mu_B H_{\text{eff}} \sum_f S_f^z \quad (6)$$

α designates one of the three space directions, namely x , y or z . The exchange interaction $J_{f,g}$ is assumed to be non-zero only for first neighbouring sites f and g , and to have the same value for each pair of nearest neighbours. The magnetic susceptibility is assumed to be uniform within the sample; the external field is also assumed to be uniform over the sample, parallel to the z axis. The field $\overrightarrow{H_{\text{eff}}}$ is the sum of the external field and of the dipole-dipole contribution which is also assumed to be uniform over the sample; so, $\overrightarrow{H_{\text{eff}}}$ is parallel to the z axis as well

as the resulting magnetization. The interesting point already noticed when dealing with the connectivity matrix is the occurrence of points of different connectivity states, as it also appears in the case of dots. In dots, external atoms, i.e. boundary atoms, have a lower number of neighbours than central atoms [25]. States of connectivity have a physical meaning in defining separate propagation areas.

The linear equation of motion for each spin reads in RPA or Tyablikov approximation [26]:

$$i\hbar \frac{d}{dt} S_f^+ = \left(\sum_g J_{f,g} \right) S_f^+ - \sum_g J_{f,g} S_g^+ + g\mu_B H_{eff} S_f^+ \quad (7)$$

Spin excitations lie in the xy plane; $S_f^+ = S_f^x + iS_f^y$.

A time Fourier-transform enables us to derive a matrix equation from:

$$S_f^+(t) = \int e^{-i\omega t} S_f^+(\omega) d\omega \quad (8)$$

In the following, we shall deal with the shifted frequency: $\omega = \hbar\omega - g\mu_B H_{eff}$

Hence, the frequencies are deduced from an eigenvalue problem:

$$\omega S_f^+(\omega) = \left(\sum_g J_{f,g} \right) S_f^+(\omega) - \sum_g J_{f,g} S_g^+(\omega) \quad (9)$$

For practical calculation, all non-zero exchange integrals are taken equal to unity and there is no external field which would just shift the frequencies. With this field value, the frequency of the uniform mode is zero. So, the set of equations (9) is just defined by the set topology. It is solved numerically for the considered Sierpinski Carpets as introduced previously. Eigenvalues of equations (9), i.e. spin wave frequencies, as well as normalized eigenvectors, i.e. spin wave profiles, are calculated numerically by means of the QR algorithm implemented in the LAPACK computational library.

2.3.2. The spin wave frequencies

In a Sierpinski Carpet $SC(n,p,k)$, there are $N = p^k = n^{kd_f}$ sites and so n^{kd_f} spin wave modes of frequencies ω_i . Hence, the normalized integrated density of states (NIDOS) reads:

$$F(\omega) = n^{-kd_f} \sum_i Y(\omega - \omega_i) \quad (10)$$

$Y(x)$ is the Heaviside step function [27]. NIDOS enable us to compare density of states of sets with different fractal dimensions and different numbers of iteration steps, on the same frequency scale and on the same ordinate scale. The boundaries of the variation of the frequency ω are zero for the uniform mode and eight for the highest frequency mode of a

“full” Sierpinski Carpet (with dimensional space equal to 2) from equation (9). These limits are observed in Fig. 7 where the NIDOS of a “full” Sierpinski Carpet SC(5, 25, 3) is compared to the NIDOS of a Sierpinski Carpet SC_a(5, 24, 3) with a central missing square ($d_f \approx 1.975$) and to the NIDOS of SC_a(5, 16, 3) with nine central missing squares ($d_f \approx 1.723$). These sets are taken at the same level of iteration. This comparison enables us to understand the consequences of a fractal nature on excitation spectrum.

2.3.3. The singular continuous NIDOS of fractal sets; effect of the fractal dimension.

The NIDOS's shown in Fig. 7 contain respectively 15 625, 13 824 and 4 096 points, i.e. a very large number of points which would lead to a continuous curve for a regular distribution as observed for the full set SC(5, 25, 3); moreover, the linear size of these three structures is the same ($L=125$). For a full set as SC(5, 25, 3), a space Fourier transform defines the wave vectors k and equation (9) becomes a dispersion relation [28] between frequency and wave vector. The two-dimensional wave vector quantification on k implies that the mode number grows as a quadratic function of the wave vector amplitude: $N = C'k^2$. The classical dispersion relation reads: $\omega = 8\sin^2(k/2)$ where each spin has four neighbours [28]. The NIDOS of the full set SC(5, 25, 3) is well seen on Fig. 7 to be nearly perfectly continuous, in agreement with the equation deduced from the previous dispersion relation:

$$N = C \left[\text{Arc sin} \left(\frac{\omega}{8} \right)^{1/2} \right]^2 \quad (11)$$

For low frequencies, at leading order, the integrated density of states of the full set increases linearly with the frequency as seen on Fig. 7, and as obvious from the last formula. With this large number of points, all the NIDOS of the true fractal sets with $d_f < 2$ shown in Fig. 7 appear to be singular continuous functions. Such a singular continuous behaviour of the excitation spectrum has already been observed in incommensurate structures [29] as well as for aperiodic systems associated with Fibonacci series [30]. The name devil's staircase was associated with such spectra. In the latter systems, self-similar hierarchical effects occur; so, this singular continuous behaviour seems associated with self-similarity. Here, the devil's staircase [29, 30] aspect of NIDOS is due to the occurrence of both large steps and very steep cliff-like variations. The large NIDOS steps mean the existence of large gaps in the energy spectrum as they also occur in magnonic spectra [31, 32], and the very steep cliff-like NIDOS

variations are due to the existence of nearly (or exactly) degenerate modes with nearly (or exactly) the same frequency. Since high frequency modes are still present, cliffs of degenerate modes are necessarily associated with depletion areas in the spectrum, i.e. steps. These properties are general for deterministic fractal sets. It is worth noticing that higher order singularities occur in the NIDOS.

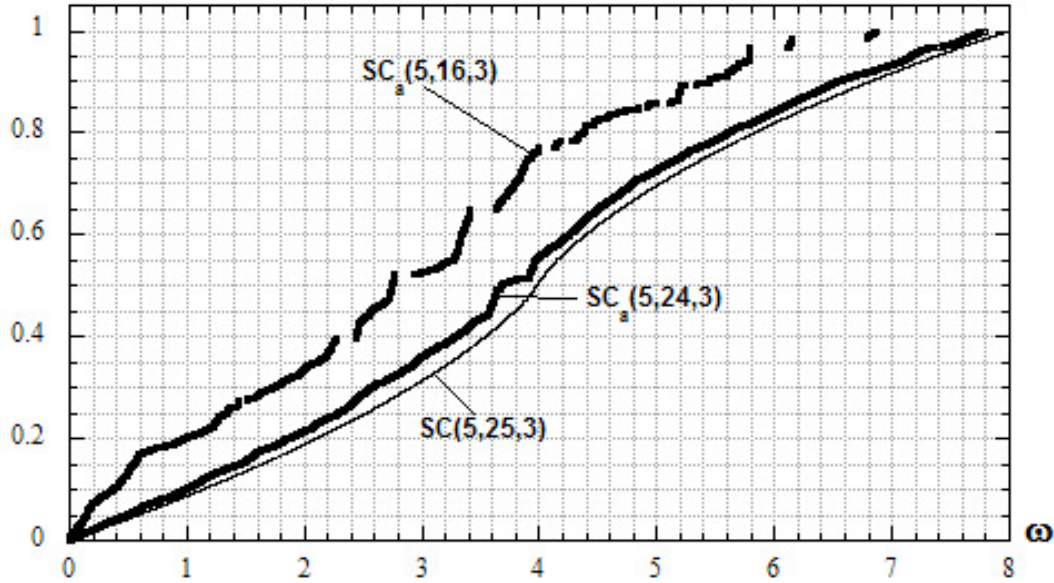
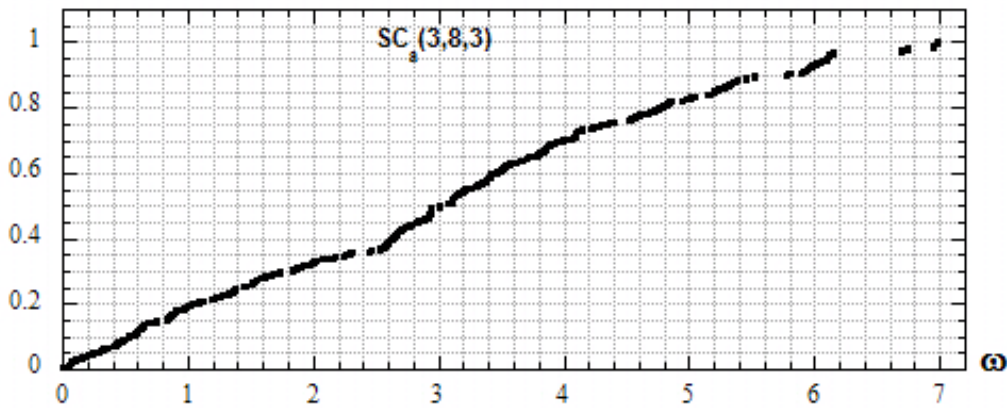


Fig. 7. The compared normalized integrated density of states (NIDOS) of $SC(5, 25, 3)$, $SC_a(5, 24, 3)$ and $SC_a(5, 16, 3)$. Note that true fractal sets have singular continuous NIDOS with singularities located at well defined frequencies, namely 0.6, 1.4, 2.3, 2.8 and so on in the case of $SC_a(5, 16, 3)$.

In the case of more complex and less symmetric fractal structures, the existence of different connectivity areas is still responsible for an excitation spectrum splitting as it appears in layered materials [33]. In each case there is an extra excitation spectrum splitting between these different parts. Since numerous nearly independent bands of states are quite similar parts, there are also approximate degeneracy properties of the excitation spectrum, i.e. NIDOS cliffs. So, NIDOS are expected to be singular continuous for all fractal sets. Fig. 7 also shows that, when the fractal dimension decreases, i.e. when the lacunarity increases, NIDOS is shifted upwards. This effect is due to the reduction of the number of low energy modes, i.e. collective modes, because of the lacunarity: In systems with large voids, smoothly varying modes are not so easy to be produced as in regular periodic lattices. This difficulty for

obtaining low frequency modes is characteristic of fractals. So fractal spectra are shifted towards high frequencies.

The very singular continuous nature of NIDOS for a fractal set is well shown in Fig. 8 where different levels of iteration of the same Sierpinski Carpet are compared, namely $SC_a(3, 8, 3)$, $SC_a(3, 8, 4)$ and $SC_a(3, 8, 5)$ where the fractal dimension is $d_f \approx 1.893$. Even with this rather high fractal dimension, singularities appear at all iteration levels. The spectra of Fig. 8 involve respectively 512, 4 096 and 32 768 modes. A more detailed analysis of finite size effects is provided in Fig. 9 and shows that the essential singular nature of NIDOS is more and more easily seen when the iteration step is increased. A thorough analysis of the evolution of the NIDOS with the iteration step k in the vicinity of gaps clearly shows that several of these gaps survive the increase in the structure size. Four gaps are analyzed here: close to $\omega=3$, close to $\omega=4$, close to $\omega=4.9$ and close to $\omega=6.2$. In these three cases, the existing steps are confirmed by a higher iteration level: The convergence of the gaps widths towards a non zero value is easily seen on these figures. Moreover, more degenerate modes are found when the iteration level is increased. So, it clearly turns out that this singular continuous nature cannot be a numerical artefact: This feature is peculiar to fractal systems.



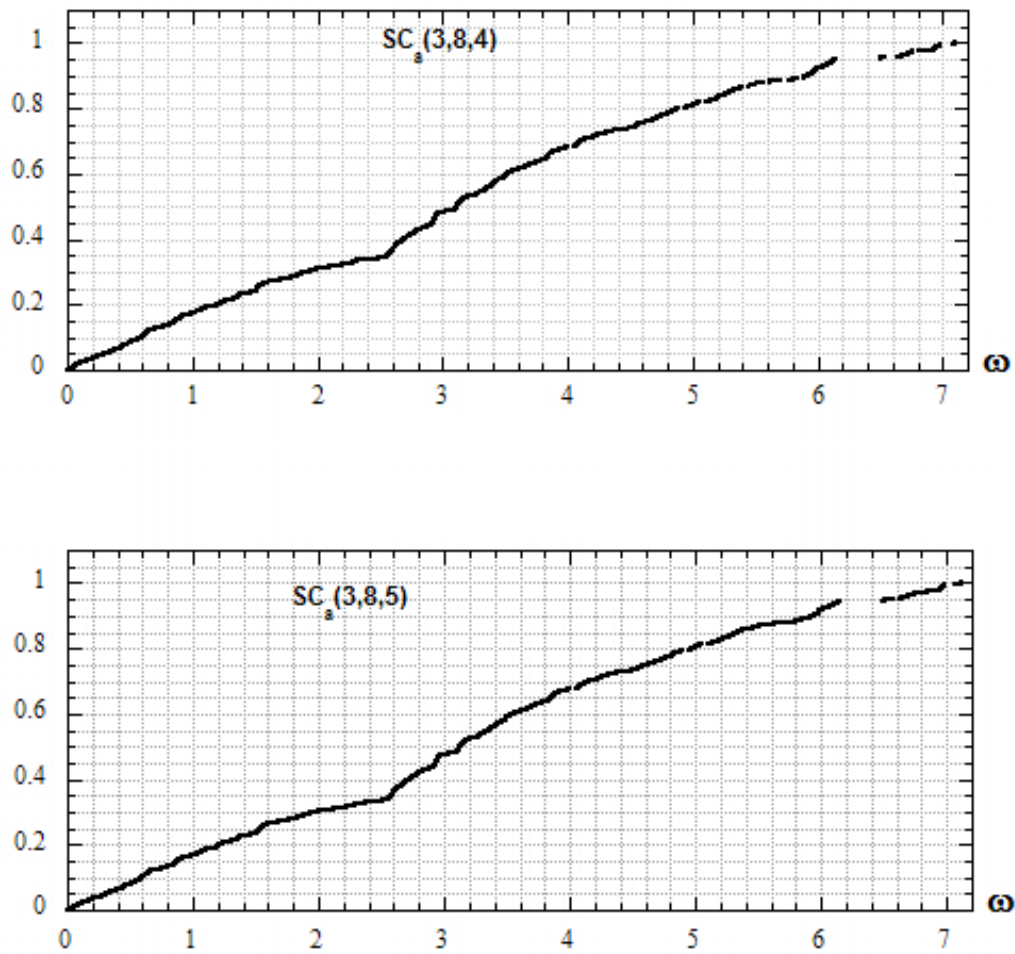


Fig. 8. Compared NIDOS of $SC_a(3, 8, k)$, with $k=3,4,5$. Note the persistence of steps and cliffs with the increase in the structure size.

This basic singular continuous nature of the excitation spectrum of fractals can be understood from the fact that the density of these fractals (with respect to the embedding space, namely 2) decreases when the number of iteration steps is increased; thus, collective modes are harder and harder to be established while more and more parts of fractal sets become nearly independent and thus are responsible for nearly degenerate modes.

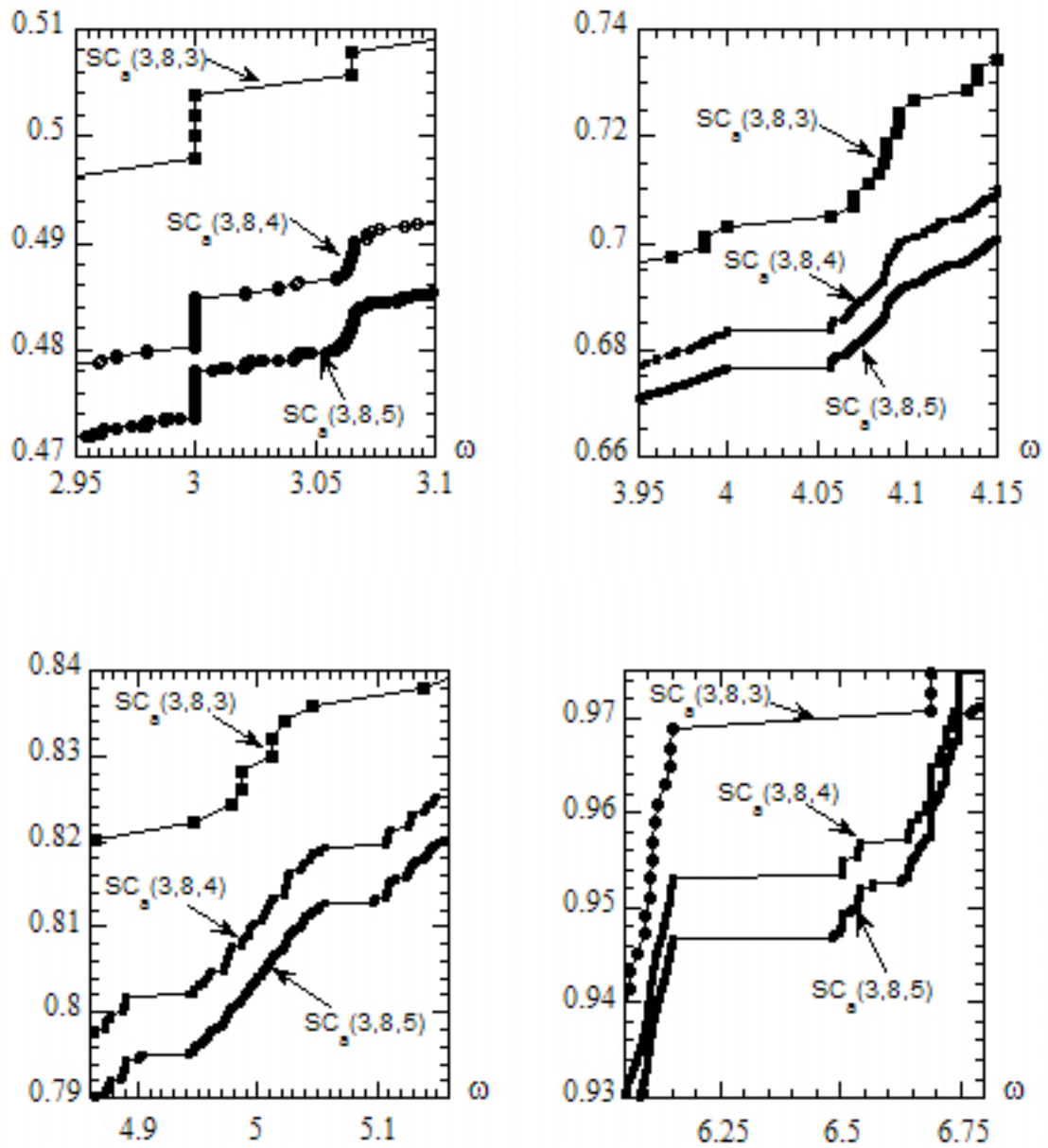


Fig. 9. Details of compared NIDOS of $SC_a(3,8,k)$ with $k=3,4,5$.

2.3.4. Topology effect on NIDOS at a given fractal dimension.

Topology effects on NIDOS are observed here by comparing NIDOS for fractal sets of the same dimension and the same level of iteration but with different topology. This is the case shown in Fig. 10 where the NIDOS of $SC_a(4, 12, 4)$ and $SC_b(4, 12, 4)$ are compared. The generating cells of these structures were already reported in Fig. 3 and their common fractal

dimension is: $d_f = 1.792$. These singular continuous functions NIDOS contain 20 736 modes each and are quite distinct from each other.

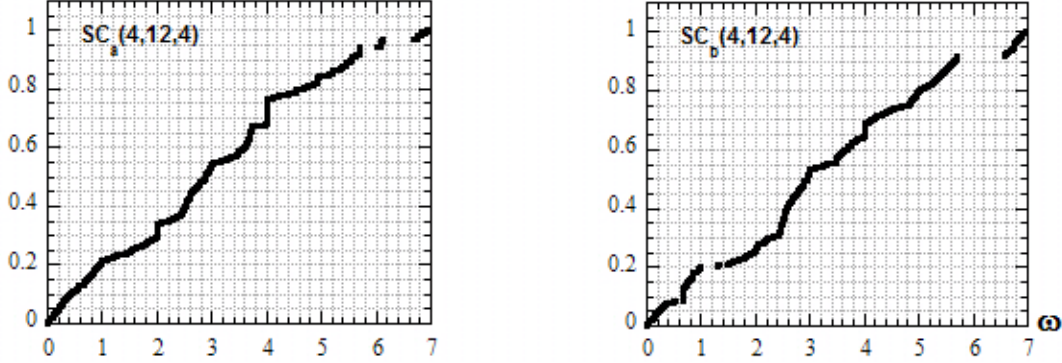


Fig. 10. NIDOS of $SC_a(4, 12, 4)$ and $SC_b(4, 12, 4)$. Note the different location of steps and cliffs.

The $SC_a(4, 12, 4)$ NIDOS lies upper than the other one. This is mainly due to the existence of more numerous long wavelength modes in $SC_a(4, 12, 4)$ than in $SC_b(4, 12, 4)$. Numerous full straight lines appear through $SC_a(4, 12, 4)$ as noticed from Fig. 3 and confirmed from the first subdimension $d_I=1$ of the associated connectivity matrix of equation (1). Reversely, for $SC_b(4, 12, 4)$ instead of full lines, there are only broken lines, i.e. Cantor sets with the subdimension $d_I=1/2$ of the connectivity matrix of equation (2). Another effect of the connectivity differences between these two structures is seen at low frequency where several steps and cliffs appear for $SC_b(4, 12, 4)$ NIDOS, without their counterpart in $SC_a(4, 12, 4)$ NIDOS. This is due to the bad propagation of smooth waves through $SC_b(4, 12, 4)$ as a consequence of this weak connectivity.

So, connectivity variations have strong consequences on excitation spectrum. This leads us to consider larger values of the size n of the generating cell in order to produce several symmetric configurations with the same fractal dimension, and test carefully the NIDOS sensitivity to topology, i.e. connectivity. This is the case for the Sierpinski Carpets generated by the cells shown in Fig. 4: $SC_a(5, 16, 1)$, $SC_b(5, 16, 1)$ and $SC_c(5, 16, 1)$. The structures have a common fractal dimension $d_f \approx 1.723$ but different first connectivity subdimensions: a) $d_I=1$ b) $d_I=0.431$ and c) $d_I=0.683$. The NIDOS of these three Sierpinski Carpets at the third iteration step, $SC_a(5, 16, 3)$, $SC_b(5, 16, 3)$ and $SC_c(5, 16, 3)$ are compared in Fig. 11.

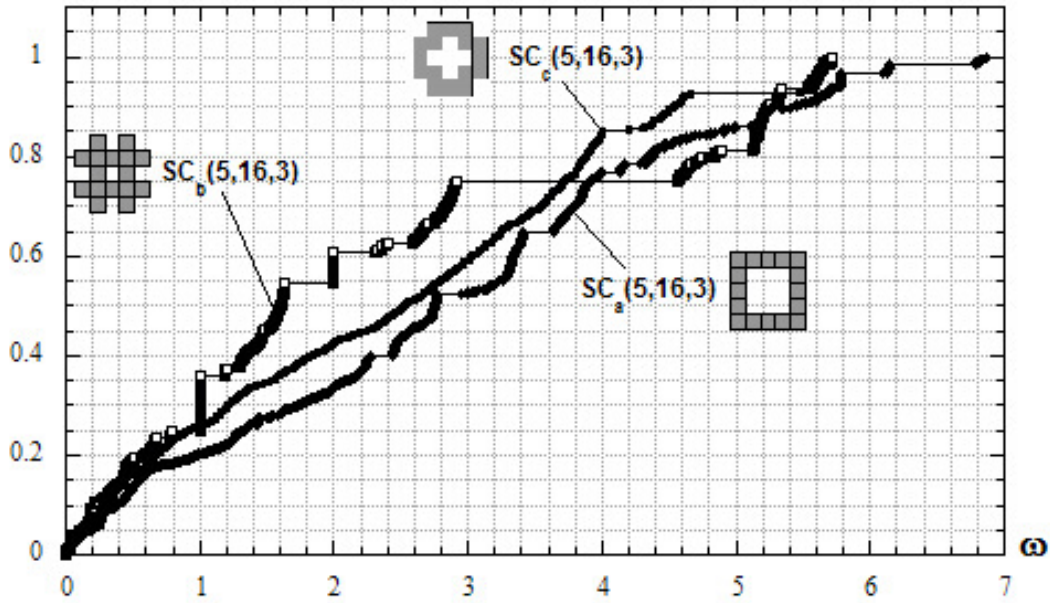


Fig. 11. The NIDOS of $SC_a(5, 16, 3)$, $SC_b(5, 16, 3)$ and $SC_c(5, 16, 3)$ with a common fractal dimension $d_f \approx 1.723$.

These three NIDOS have quite different singular continuous behaviours in the whole frequency range. As already noticed above for $SC_a(4, 12, 4)$ compared to $SC_b(4, 12, 4)$ at low frequencies, the upper NIDOS is associated with the highest connectivity subdimension, i.e. with $SC_a(5, 16, 3)$. This is well shown in the two zooms reported on Fig. 12. Furthermore, Fig. 11 also confirms NIDOS singular continuous nature, even at low frequencies. The fractal structure with the lowest connectivity subdimension, i.e. $SC_b(5, 16, 3)$ gives the NIDOS which contains the largest number of steps and cliffs. This is well in agreement with the fact that this structure involves many more or less independent blocks. The intermediate structure, $SC_c(5, 16, 3)$, is rather compact and its NIDOS exhibits less steps and cliffs than others, for intermediate frequencies. This direct comparison of NIDOS for different structures shows how NIDOS is sensitive to topology as well measured by connectivity subdimensions. It must be added that the compact appearance of $SC_c(5, 16, 3)$ can be distinguished from other configurations by looking at connectivity properties including next nearest neighbours. As a matter of fact the notion of connectivity generates a full set of connectivity matrices at different ranges. And finally the full set of these connectivity matrices and thus of connectivity eigenvalues and subdimensions gives a sharp view of topology in fractal structures.

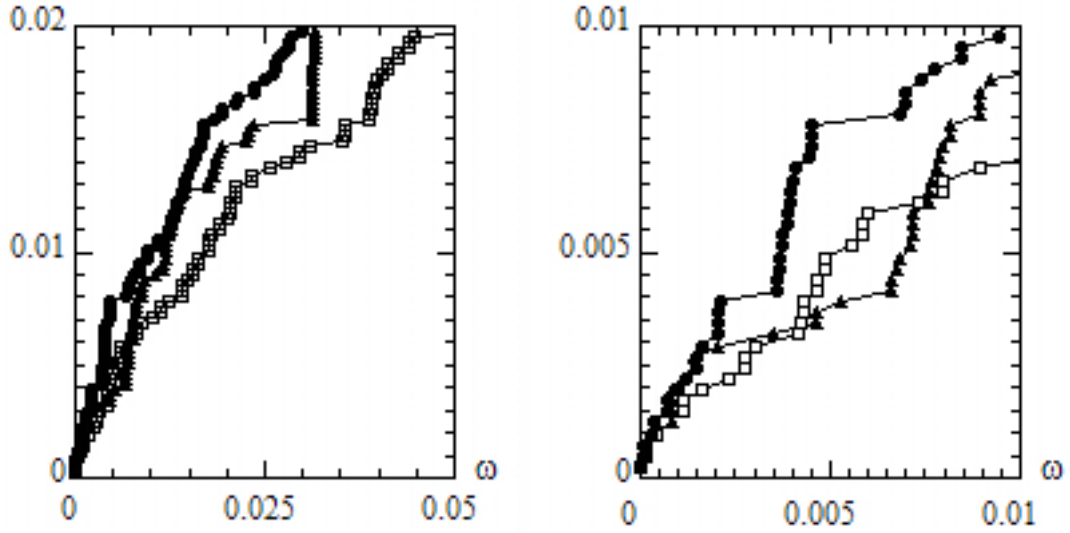


Fig. 12. Two Zooms on the low frequency part of Fig. 11. Note the occurrence of low frequency gaps and the higher position of the NIDOS of $SC_a(5, 16, 3)$.

Several typical cases of excitation spectra have been investigated, and the general results are the singular continuous nature of NIDOS as well as the strong sensitivity of excitation spectra to structural topology, as observed and measured by connectivity subdimensions. Since eigenvectors are more sensitive than eigenvalues to the details of the dynamic matrix, i.e. to the details of the equations of motion, the analysis of spin wave modes in fractals follows quite naturally.

2.3.5. Spin wave modes: Localization and symmetry

Since each NIDOS contains several thousands of modes, it is not possible to consider here several structures, and it is not even possible to consider all distinct modes of a single structure. The present introductory analysis comes from the detailed study of the 4096 modes of the Sierpinski Carpet $SC_a(3, 8, 4)$. This structure is rather dense, with a fractal dimension $d_f \approx 1.893$. The number of iteration steps is large enough to ensure an actual fractal structure as observed on NIDOS in Fig. 7 and 8. The whole analysis reveals two main points for these spin wave profiles: localization and symmetry. Localization is expected to occur because of the existence of different connectivity areas, which can act as different media. And in these symmetric fractal structures, spin waves also have symmetric properties.

2.3.5.a. Localization.

As accounted from the rank of the connectivity matrix in equation (4), four distinct levels of connectivity appear in $SC(3, 8, 4)$ when starting from an isolated $SC(3, 8, 1)$: sites with two orthogonal bonds, sites with two collinear bonds, sites with three bonds and sites with four bonds. The eigenvectors calculated from the QR algorithm provide the amplitudes of the associated spin waves at each occupied site, and are normalized to unity. The visualization of each mode is done by representing the local spin wave intensities according to a scale of grey levels: white colour is associated to a zero intensity, while black is associated to the maximum intensity of the mode. In this way, nodal curves of the waves, i.e. low intensity points, enable a convenient visualization of the modes since they appear clearer; moreover the unoccupied sites of the embedding two-dimensional plane of the Sierpinski Carpet are white. Modes are classified according to their frequency by increasing order when starting from the lowest frequency. As already pointed out, the first mode has zero for frequency and is uniform over the sample. So, the first low energy modes have a smooth intensity variation over the sample as observed in Fig. 13, 14 and 15. Mode number 2 is reported in Fig. 13 with evidence for the underlying $SC(8, 3, 4)$ structure which was not reported before. Its nodes are located close to a curved large diagonal line. There is a weak deviation from the diagonal line near external corners, where intensities are quite low. This mode has a twofold central symmetry. Of course mode number three, not shown here, has a nodal line located near the first diagonal and has also a central twofold symmetry.

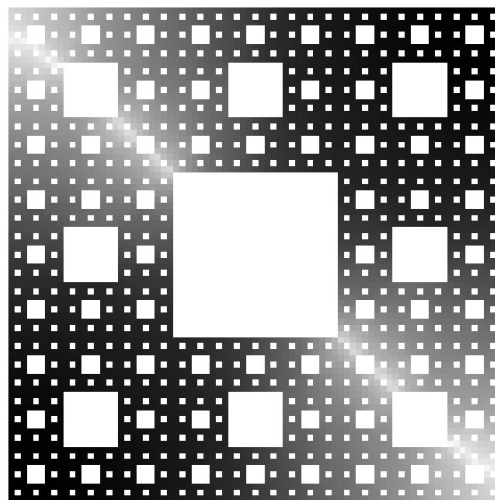


Fig. 13. Mode number 2. Note its nodal curve along the diagonal.

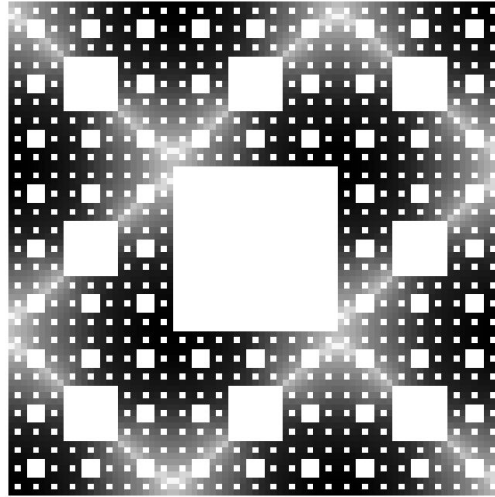


Fig.14. Mode 10. Note the 5 diagonal nodal curves defining 8 zones.

Fig. 14 shows the mode number 10, another low frequency mode. Once more it exhibits a twofold central symmetry. Five nodal lines appear on this spin wave profile. All these nodal lines are parallel to square diagonals and are pinned by the corners of large missing squares. The partition in eight zones evidenced in Fig. 14 underlines the last iteration step of the underlying structure with nodal diagonals cutting the edge at one or two thirds. These nodal lines go diagonally through the eight large holes of the previous segmentation step. Clearly spin waves take advantage of the hierarchical structure and of the underlying symmetries. Similar remarks are also valid for the mode number 100 which is shown in Fig. 15. This mode shows a fourfold symmetry with four thin nodal lines which are located at the large diagonals. A careful look at Fig. 15 shows a nearly circular structure with one peak located in the vicinity of a ring near the large central hole and a larger annular area of high amplitude connecting the second largest holes. Nearly three large amplitude rings can be distinguished as well as parts of three low amplitude rings. In this case, there is a resemblance with modes located within a large annular ring, provided by a ‘full’ two-dimensional structure.

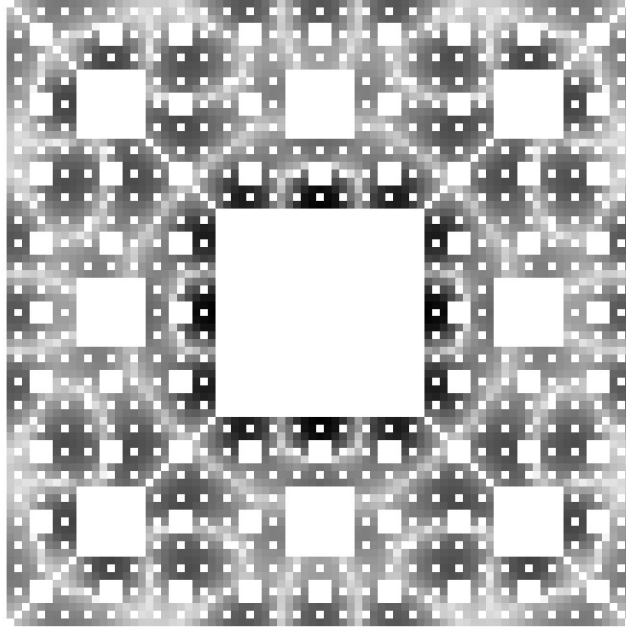


Fig. 15. Mode 100. Note the fourfold partition

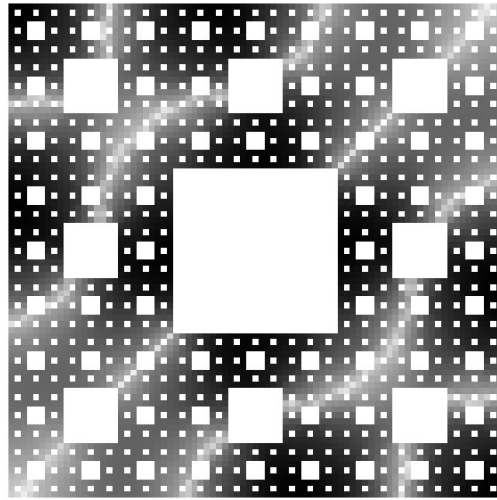


Fig. 16. Mode 15. Note the twofold symmetry and curvature of the nodal curve.

Fig. 16 shows mode 15 which exhibits a twofold symmetry and a similar tendency towards curved structures, with nodal curves pinned on large missing squares. In these fractal structures with a rather high density, (here at this iteration step the density is $d = 0.62$) these low frequency eigen-modes are not so far from modes of a full part of a lattice. Moreover, these modes take also advantage of the location of holes in an optimal way.

About localization, an interesting feature comes from the analysis of successive spin wave modes around a set of degenerate modes, i.e. a cliff in the NIDOS. There is a strong

geometrical change of intensities distribution between these modes. This is shown here in Fig.17 and Fig. 18 where spin wave mode numbers 1966 and 1967 are reported respectively. These modes have respective frequencies $\omega = 2.9795$ and $\omega = 3$. Twenty degenerate modes follow, namely from 1967 to 1986, at exactly the same frequency $\omega = 3$, as it can be seen on Fig. 9a. The next mode 1987 has $\omega = 3.0211$ for frequency. Modes 1966 and 1967 exhibit both twofold symmetry, but their localizations are quite different. Mode 1966 is quite extended while mode 1967 is located on a few diagonal lines built up from 3-bonds sites and 4-bonds sites resulting in a kilim-like carpet. The twenty modes from 1967 to 1986 share the same basic localization.

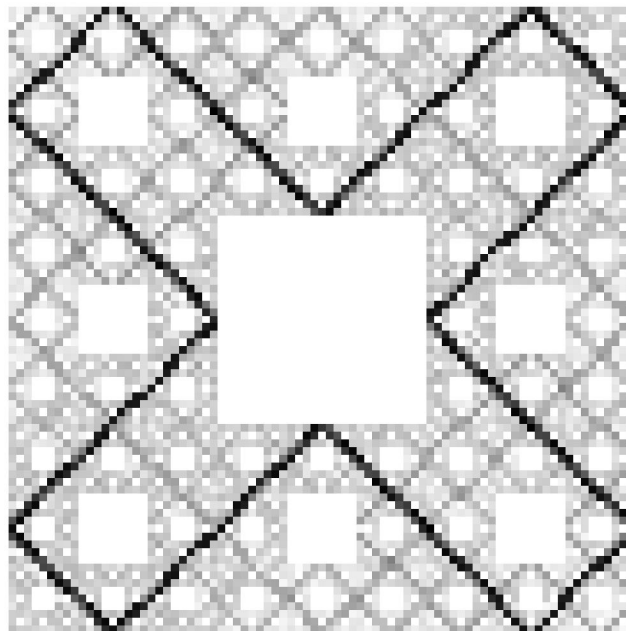


Fig. 17. Mode 1966. Note the twofold symmetry and the extension.

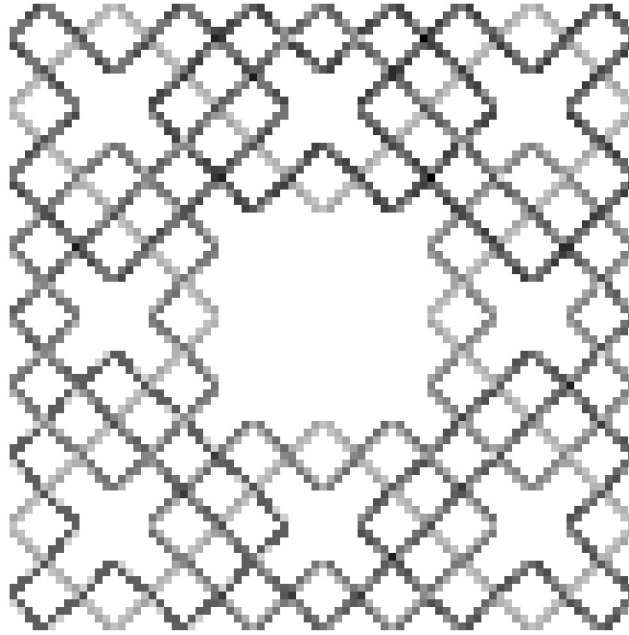


Fig. 18. Mode 1967. Note the localization.

In Fig. 17 a large X cross appears on a rather high level of excitation in the whole sample, while in Fig. 18, the excitation is just located within a few lace lines. For modes 1967 to 1986, the excitation is restricted within the same lines which are essentially made of 3-bonds sites. For mode 1987, not represented here, the excitation extends over the whole sample and on a lace of diagonals, rather similarly to what occurs for mode 1966.

2.3.5.b Symmetry

Fig. 13-18 already exhibit different levels of symmetry within the square: twofold central symmetry and fourfold symmetry. As a matter of fact the twenty degenerated modes of frequency $\omega = 3$, whose mode number run from 1967 to 1986, exhibit symmetry within a lace as shown here in Fig.19 where mode number 1977 is represented; moreover, it should be noticed that the lowest, already zero intensities are located at the same places for all these modes, i. e at the corners of the holes. For mode 1977 the spin wave amplitude is lower on the right side than in the other parts while for mode 1967 shown in Fig. 18, the spin wave amplitude is lower close to the left down corner than in the other parts. So these degenerate spin wave states show symmetric variations within a lace.

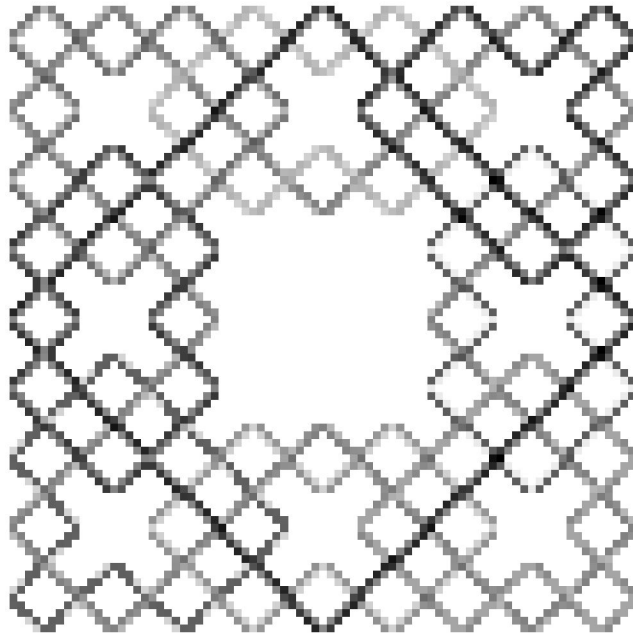


Fig. 19. Mode 1977. Note the low amplitudes on the right side.

Another symmetric appearance is observed among these modes linked with linear structures reminding the so-called ‘channelling modes’ associated to vibrational states [13] parallel to the sides of the Carpet (and not along the diagonals); such a mode is shown in Fig. 20 for mode number 3904 which appears at $\omega = 6.15$ just before the large gap observed on Fig. 9 and which leads to the next value $\omega = 6.5027$ for the mode 3905.

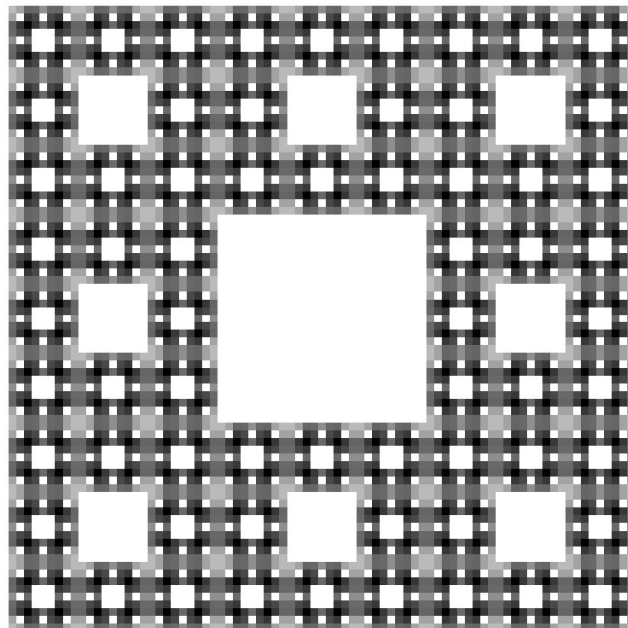


Fig. 20. Mode 3904. Note the fourfold tartan-like symmetry

3. Comments and Conclusions

Numerous extensions of this work on spin waves in fractals can be achieved. Spin wave profiles can be studied for different fractals. This work should also be completed to include random fractals. Then spin wave modes could be used to understand magnetic properties of these systems. Finally other excitation spectra must be considered in a similar way. So some simple extrapolations of the present work can be useful to introduce such generalizations.

3.1. Spin waves in random fractal structures.

The main features observed in deterministic simple fractal sets are the occurrence of many gaps and degeneracy in the spin wave spectrum. Gaps must also appear for random fractal structures since the existence of several connectivity areas leads to a general splitting of the spectra. Since these structures are less symmetric, there will be only partial degeneracy between more or less localized modes in different parts. So, NIDOS cliffs of random fractals are expected to be smoother than these of deterministic fractals. Similarly, symmetry properties are less obvious in random fractals than in deterministic ones. However localization properties in areas of well defined connectivity are expected to remain.

3.2. Magnetic properties of fractals.

For thermal properties of magnetization, low frequency modes are preponderant. From Fig.11 and Fig. 12, it appears that low frequency modes are quite sensitive to topology. So, the thermal variations of magnetization in fractals are expected to be very sensitive to fractal topology. This is confirmed by the calculations of critical exponents in fractals which are already known to be sensitive to fractal topology [16-17]. About magnetization reversal of fractal sets, a similar dependence on topology is obvious since topology acts upon the whole spectra. For magnetization resonance the present calculation would lead to a single uniform mode. However the presence of anisotropy lifts this degeneracy [25, 28] and thus several modes are expected to be observed. Long wavelength modes are the more important for full samples, and these low frequency modes are perturbed by the fractal structure as shown in Fig. 12. So, for exchange modes, different modes are expected to be observed by magnetic resonance, mainly because of the existence of several connectivity areas which make the fractal set acting as a multilayered sample. As a matter of fact long range interactions between spins must also be accounted for, with the examples of RKKY and dipolar forces.

Competition between such long ranged interactions and the intrinsic long ranged fractal structure defines a very difficult problem.

3.3. Other excitation spectra in fractals

The singular continuous nature of NIDOS must also occur for electrons and phonons in fractals, since calculations on dynamical matrix or tight binding matrices are quite similar to the ones used here about spin waves with local exchange bonds. The existence of many gaps in the electronic bands leads first to stabilize structures with full occupied bands and subbands. So, weak gaps are expected to occur. As a consequence, there will be a rather bad conduction in fractals as it occurs for semiconductors or quasicrystals. On the other hand the existence of degeneracy, i.e. cliffs in the NIDOS, leads to increase conductivity properties as it occurs in semimetals. Since gaps are rather weak, non linear properties can also occur. So there is a rich domain to explore. About elastic waves in fractals, the present results suggest that sound propagation in fractals will be a rich topic with forbidden bands for instance.

References

1. H. Brune, Surf. Sci. Rep. **31**, 121 (1998).
2. JM Hammersley, Ann. Math. Statist. **28**, 790 (1957); G.R. Grimmett, “*Percolation*”, Springer Verlag, Berlin (1989).
3. T. A. Witten, L. M. Sander, Phys. Rev. Lett. **47**, 1400 (1981); R. Ball, M. Nauenberg, T. A. Witten, Phys. Rev. A **29**, 2017 (1984); T.R. Ni Mhiochain and J.M.D. Coey, Phys. Rev. E **69**, 061404 (2004); O. Praud and H.L. Swinney, Phys. Rev. E **72**, 011406 (2006); A.N. Gupta and H.B. Bohidar, Phys. Rev. E **76**, 051912 (2007).
4. B.B. Mandelbrot, “*Fractals: Form, Chance and Dimension*” W.H. Freeman, San Francisco (1977); “*The fractal geometry of nature*” W.H. Freeman, San Francisco (1982).
5. S. Alexander and R. Orbach, J. Phys. (Paris) **43**, L625 (1982); R. Rammal and G. Toulouse, J. Phys. (Paris) **44**, L13 (1983).
6. G. Cantor, Acta Mathematica **4**, 381 (1884).
7. F. Hausdorff, Math. Annal. **79**, 157 (1919) A. S. Besicovitch, Math. Annal **101**, (1929).
8. R. Calemczuk, A.M. De Goer, B. Salce, R. Maynard and A. Zarembovitch, Europhys. Lett. **3**, 1205 (1987); J. Pelous, M. Foret, A. Chougrani and R. Vacher, Philos. Mag. **65**, 339 (1992).

9. A. Ghazali and J.-C.S. Levy, Phys. Rev. E **69**, 061405 (2004).
10. Y. Gefen, B.B. Mandelbrot and A. Aharony, Phys. Rev. Lett. **45**, 855 (1980).
11. M. Perreau and J.-C.S. Levy, Phys. Rev. A **40**, 4690 (1989); Physica A **157**, 31 (1989); P. Monceau, J.-C.S. Levy and M. Perreau, Phys. Lett. A **171**, 167 (1992).
12. S.N. Evangelou, Phys. Rev. B **33**, 3602 (1986); R.B. Stinchcombe and I.R. Pimentel, J. Phys. A **21**, L807 (1988); S.N. Kaul and S. Srinath, Phys. Rev. B **63**, 094410 (2001).
13. P.J.-M. Monceau and J.-C.S. Levy, Phys. Rev. B **49**, 1026 (1994).
14. M. Kohmoto, L.P. Kadanoff and C. Tang, Phys. Rev. Lett. **50**, 1870 (1983); S. Aubry, C. Godreche and J.M. Luck, Europhys. Lett. **4**, 639 (1987); J.M. Luck, Phys. Rev. B **39**, 5834 (1989).
15. R. Penrose, Eureka, **39**, 16 (1978); S. Benakli, D. Mercier and J.-C.S. Levy, this volume.
16. P. Y. Hsiao, P. Monceau, and M. Perreau, Phys. Rev. B **62**, 13856 (2000); P. Monceau and M. Perreau, Phys. Rev. B **63**, 184420 (2001); P. Y. Hsiao and P. Monceau, Phys. Rev. B **65**, 184427 (2002); P. Monceau and P. Y. Hsiao, Physica A, **331**, 1 (2004).
17. P. Y. Hsiao and P. Monceau, Phys. Rev. B, **67**, 064411 (2003); P. Monceau and P. Y. Hsiao, Recent Research Developments in Physics, **5**, 903 (2004) Transworld Research Network, Kerala.
18. M.N. Baibich *et al.* Phys. Rev. Lett. **61**, 2472 (1988); M. Vohl *et al.* Phys. Rev. B **39**, 12003 (1989); J. Shen, IEEE Trans. Magn. **33**, 4492 (1997).
19. T.G. Rappoport, P. Redlinski, X. Liu, G. Zarand, J.K. Furdyna and B. Janko, Phys. Rev. B **69**, 125213 (2004); R. Plachy, K.I. Pokhodnya, P.C. Taylor, J. Shi, J.S. Miller and A.J. Epstein, Phys. Rev. B **70**, 064411 (2004).
20. M.A. Ruderman and C. Kittel, Phys. Rev. **96**, 99 (1954).
21. L.D. Landau and E.M. Lifshitz, “*The Classical Theory of Fields*” Pergamon Press, Oxford, 119 (1970).
22. P. Bergero, F. Peruani, G. Solovey, I. M. Irurzun, J. L. Vicente, and E. E. Mola, Phys. Rev. E **69**, 016123 (2004).
23. A. Di Carlo, P. Vogl and W. Pötz, Phys. Rev. B **50**, 8358 (1994).
24. V.V. Kruglyak, R.J. Hicken, J. Magn. Magn. Mater. **306**, 191 (2006); L. Dobrzynski *et al.*, this volume.
25. J.-C.S. Levy, M. Krawczyk and H. Puzkarski, J. Magn. Magn. Mat. **305**, 182 (2006).

26. S.V. Tyablikov, « *Methods in the Quantum Theory of Magnetism* » Plenum Press, New York (1967); R.E. de Wames and T. Wolfram, Phys. Rev. **185**, 720 (1969).
27. “*Handbook of Mathematical Functions*” Eds. M. Abramowitz and I.A. Stegun, N.B.S. Applied Mathematics Series 55 (1964).
28. C. Kittel, Phys. Rev. **110**, 1295 (1958).
29. P. Bak, Phys. Rev. Lett. **46**, 791 (1981).
30. R. Merlin, K. Bajema, R. Clarke, F.-Y. Juang and PK Bhattacharya, Phys. Rev. Lett. **55**, 1768 (1985).
31. M. Krawczyk, J.-C.S. Levy, D. Mercier and H. Puszkarski, Phys. Lett. A **282**, 186 (2001).
32. M. Krawczyk and H. Puszkarski, this volume, L. Dobrzynski et al. this volume.
33. M. Krawczyk, H. Puszkarski, J.-C.S. Levy and D. Mercier, J. Phys.: Condens. Matter **15**, 2449 (2003).